Flinders UNIVERSITY

Start-up plane Poiseuille flow of a Bingham fluid

Raja R. Huilgol, Andreas N. Alexandrou, Georgios C. Georgiou

PII: S0377-0257(18)30257-X
DOI: https://doi.org/10.1016/j.jnnfm.2018.10.009
Reference: JNNFM 4058

To appear in: *Journal of Non-Newtonian Fluid Mechanics*

Received date: 26 July 2018
Revised date: 15 October 2018
Accepted date: 26 October 2018

Please cite this article as: Raja R. Huilgol, Andreas N. Alexandrou, Georgios C. Georgiou, Start-up plane Poiseuille flow of a Bingham fluid, *Journal of Non-Newtonian Fluid Mechanics* (2018), doi: https://doi.org/10.1016/j.jnnfm.2018.10.009

Highlights

- The start-up plane Poiseuille flow of a Bingham fluid is considered.
- The analytical expression for the velocity in the core is given.
- The analytical solution is extended to include the velocity in the yielded zone.
- Strict bounds on the validity of the analytical solution are provided.

Start-up plane Poiseuille flow of a Bingham fluid

Raja R. Huilgol,[a] Andreas N. Alexandrou,[b†] and Georgios C. Georgiou[c]

[a] College of Science and Engineering, Flinders University, GPO Box 2100, Adelaide SA 5001, Australia
[b]Department of Mechanical and Manufacturing Engineering, University of Cyprus, PO Box 20537, 1678 Nicosia, Cyprus
[c]Department of Mathematics, University of Cyprus, PO Box 20537, 1678 Nicosia, Cyprus

1 Introduction

In non-Newtonian fluid mechanics, analytical solutions of initial-boundary value problems are very rare. When one considers the flows of a Bingham fluid, only four are known. Three of them were found by Safronchik [1, 2, 3], and the other by Sekimoto [4]. The problem of interest here is the solution to the start-up flow in a channel, or the plane Poiseuille flow [1]. It is assumed that at $t = 0^+$, a constant non-dimensional pressure drop per unit length $G > 0$ is suddenly applied and the Bingham fluid is set in motion. The yield surface moves into the fluid from the upper and lower planes of the channel and a core forms in the interior. This core region continues to shrink until the flow becomes steady. The solution to the problem requires both the velocity field as well as the location of the yield surface $\delta(t)$ be found at any given time t. Safronchik's method [1] delivers these results for a finite period of time only due to the way the solution has been constructed; for a detailed description of the method and its limitations, see Huilgol [5].

Since the location of the yield surface at $y = \delta(t)$ has to be found from the solution of a nonlinear integral equation, an approximate solution valid for a short period of time only can be derived. In Section 2, Safronchik's method [1] is revisited and the result for $\delta(t)$ is given by Eq. (2.15), and the velocity $u_c(t)$ of the core appears in Eq. (2.18) and its time of validity t_1 is given by Eq. (2.19). If one assumes that the velocity $u_c(t)$ in the core is an increasing function of time till the flows becomes steady, a different upper bound t_2 for the period of approximation arises; see Eq. (2.20). Finally, a

third bound t_3 can be derived if the size of the core is assumed to shrink and approach its final value when the flow is steady; see Eq. (2.23). It is found that $t_3 < t_2 < t_1$, which means that the solution by Safronchik [1] holds over a period of time interval less than that found by him.

Next in Section 2, using the Safronchik approximation, the velocity field $u = u(y,t)$ in the yielded region can be found; see Eq. (2.26) below. This result complements the solution found in [1] and [5], where only the velocity in the core was given. It is worth noting that obtaining the analytical solution for $u = u(y,t)$ takes considerable effort. In this connection, one notes that three integrals, $I_j(y,t),\ j = 1,2,3$, appear in the solution; see Eq. (2.24). It turns out that the last two are respectively one and two orders of magnitude less than that of the first one and can be ignored as long as the yield surface is close to the boundary of the channel. See Fig. 3, where these integrals are depicted when the Bingham number $\mathrm{Bn} = 1$ and $G = 1.2$.

In Section 3, a comparison of the velocity in the core $u_c(t)$ given by Eq. (2.18) with that obtained from $u(\delta(t),t)$ in Eq. (2.26) is made when the Bingham number $\mathrm{Bn} = 1$ and the pressure drop $G \in \{5, 10, 100\}$. It is found that these two values agree with one another as G increases.

Since the derivation of the velocity field in the yielded region is complicated, one may assume that $u(y,t)$ is parabolic and varies with time as the size of the core decreases; see Eq. (3.2). In Figs. 5 and 6, we have compared the evolution of the velocity profile in Eq. (2.26) with that in Eq. (3.2) over the time interval $[0, t_3]$. Once again, the Bingham number $\mathrm{Bn} = 1$, while $G \in \{10, 100\}$. It is found that the two profiles are similar for small t, when $G = 10$, and diverge as $t \to t_3$. The differences are greater when $G = 100$.

It is clear that the comparisons in Figs. 5 and 6 are not accurate, for the velocity field $u(y,t)$ in Eq. (2.26) is based on the assumption that $\delta(t) = 1$. Therefore, in Figs. 7 - 9, we compare the velocity profile predicted by Eq. (2.26) with the parabolic approximation of the velocity field in Eq. (3.2) over the time interval $[0, t_{09}]$, where t_{09} is the time interval when $\delta(t_{09}) = 0.9$. It is seen that the parabolic velocity approximation is adequate for small Bn/G ratios.

The Appendix describes the three integrals which appear in the velocity field in the yielded region; see Eq. (2.24). It is found that one of them can be evaluated analytically, while the other two cannot be.

2 Formulation and Solution of the Problem

2.1 The Problem

We assume that an incompressible Bingham fluid occupies a channel of width $2H$ in the $y-$direction. The flow occurs in the x-direction and is symmetric about the centreline with a velocity field $u = u(y,t)$. When the fluid has yielded, the constitutive equation for the shear stress τ in the Bingham fluid is given by

$$\tau = \tau_y + \eta \frac{\partial u}{\partial y}, \tag{2.1}$$

where τ_y is the yield stress and η is the plastic viscosity of the fluid. In the core where the fluid moves as a rigid body, the shear stress τ is not defined by a constitutive equation; rather it is bounded by the yield stress. That is $|\tau| < \tau_y$.

We consider the start-up flow of the Bingham fluid in the channel initiated by a constant pressure gradient $G > \tau_y/H$. That is, $\partial p/\partial x = -G$. The flow is divided into a yielded region $(h(t), H]$ and an unyielded one $[0, h(t)]$. In the latter, the central core moves with an unknown velocity $u_c(t)$.

Balance of linear momentum leads to the following equation:

$$\rho \frac{\partial u}{\partial t} = \frac{\partial \tau}{\partial y} + G, \quad 0 \le y \le H, \ t > 0, \tag{2.2}$$

where ρ is the density of the fluid.

In the core, while the shear stress does not satisfy a constitutive relation, its distribution is linear. That is

$$\tau = -\frac{\tau_y}{h(t)} y, \quad 0 \le y \le h(t). \tag{2.3}$$

In this core, the velocity $u = u_c(t)$ only, whence the equation of motion (2.2) reduces to

$$\frac{du_c}{dt} = \frac{1}{\rho}\left[G - \frac{\tau_y}{h(t)}\right]. \tag{2.4}$$

On integration, one finds that

$$u_c(t) = \frac{1}{\rho}\left[Gt - \int_0^t \frac{\tau_y}{h(\xi)}\, d\xi\right]. \tag{2.5}$$

Of course, $u(y,t) = u_c(t), \ 0 \le y \le h(t)$.

2.2 Non-Dimensionlisation

We shall now introduce the following non-dimensional variables, using H as the characteristic length scale and $U = \sqrt{\tau_y/\rho}$ as the characteristic velocity scale:

$$\tilde{x} = \frac{x}{H}, \quad \tilde{y} = \frac{y}{H}, \quad \tilde{t} = \frac{\eta}{\rho H^2} t, \quad \delta(\tilde{t}) = \frac{h(t)}{H}, \tag{2.6}$$

$$\tilde{u} = \frac{u}{U}, \quad \tilde{\tau} = \frac{H}{\eta U}\tau, \quad \tilde{G} = \frac{H^2}{\eta U} G. \tag{2.7}$$

Thus,

$$\frac{Gt}{\rho} = \frac{1}{\rho} \cdot \frac{\eta U}{H^2}\tilde{G} \cdot \frac{\rho H^2}{\eta}\tilde{t} = U\tilde{G}\tilde{t}. \tag{2.8}$$

Next in analogy with $t = (\rho H^2/\eta)\tilde{t}$, we let $\xi = (\rho H^2/\eta)\tilde{\xi}$, leading to

$$\frac{1}{\rho}\int_0^t \frac{\tau_y}{h(\xi)}\, d\xi = \frac{1}{\rho}\int_0^{\tilde{t}} \frac{\tau_y}{H\delta(\tilde{\xi})} \cdot \frac{\rho H^2}{\eta}\, d\tilde{\xi} = \int_0^{\tilde{t}} \frac{\tau_y H}{\eta\delta(\tilde{\xi})}\, d\tilde{\xi}. \tag{2.9}$$

Let the Bingham number be defined through $\mathrm{Bn} = \tau_y H/\eta U$. Hence, the right side becomes

$$\int_0^{\tilde{t}} \frac{\tau_y H}{\eta\delta(\tilde{\xi})}\, d\tilde{\xi} = U\ \mathrm{Bn} \int_0^{\tilde{t}} \frac{1}{\delta(\tilde{\xi})}\, d\tilde{\xi}. \tag{2.10}$$

Since $u = U\tilde{u}$, dropping the tildes for simplicity, the velocity in the core given by Eq. (2.5) takes on the following form:

$$u_c(t) = Gt - \mathrm{Bn}\int_0^t \frac{1}{\delta(\xi)}\, d\xi. \tag{2.11}$$

In the yielded region, the partial differential equation (2.2) has the form:

$$\frac{\partial^2 u}{\partial y^2} = \frac{\partial u}{\partial t} - G, \quad \delta(t) < y < 1,\ t > 0, \tag{2.12}$$

where the tildes have again been dropped. The following conditions apply:

$$u(y,0) = 0, \quad 0 \le y \le 1; \quad u(1,t) = 0, \quad t \ge 0, \tag{2.13}$$

$$\frac{\partial u}{\partial y}(\delta(t),t) = 0, \quad t > 0. \tag{2.14}$$

The required equations have now been assembled. These are Eqs. (2-12) - (2.14); their solution provides the velocity in the core (2.11), valid in $0 \le y \le \delta(t)$.

2.3 Safronchik's Solution for the Core and Time of Validity

In his important work, Safronchik [1] found that the location of the yield surface in the upper-half of the channel is given in a non-dimensional form by

$$\delta(t) = 1 - 2\alpha\sqrt{t}, \quad 0 \le t \le \frac{1}{4\alpha^2}. \tag{2.15}$$

Here the constant α is the solution of the equation

$$e^{-\alpha^2} - 2\alpha \int_{\alpha}^{\infty} e^{-s^2}\, ds = \frac{\mathrm{Bn}}{G}, \tag{2.16}$$

which can also be written as follows:

$$e^{-\alpha^2} - \alpha\sqrt{\pi}\Big[1 - \mathrm{erf}(\alpha)\Big] = \frac{\mathrm{Bn}}{G}, \tag{2.17}$$

where $\mathrm{erf}(\cdot)$ is the error function. In Fig. 1, we have depicted the way α varies with the ratio Bn/G.

The velocity in the core is given by [1]

$$u_c(t) = Gt + \mathrm{Bn}\frac{1}{\alpha}\sqrt{t} + \mathrm{Bn}\frac{1}{4\alpha^2}\ln\Big[1 - 2\alpha\sqrt{t}\Big]. \tag{2.18}$$

We see that the solutions for $\delta(t)$ and the velocity field $u = u(y,t)$ are valid provided $t < t_1$, where

$$t_1 = \frac{1}{4\alpha^2}. \tag{2.19}$$

Next, the velocity in the core, $u_c(t)$, must be an increasing function of tile till the flow becomes steady. In Eq. (2.18), by putting $du_c(t)/dt = 0$, we find that this velocity increases provided $t \le t_2$, where

$$t_2 = \frac{\Big(\sqrt{1 + \mathrm{Bn}^2/G^2} + 1 - \mathrm{Bn}/G\Big)^2}{16\alpha^2}. \tag{2.20}$$

From Eq. (2.15), we find that

$$\delta(t_2) = \frac{1}{2}\Big[1 + \frac{\mathrm{Bn}}{G} - \sqrt{1 + \mathrm{Bn}^2/G^2}\Big]. \tag{2.21}$$

Next, the width of the rigid core when the flow is fully developed is given by

$$\delta_\infty = \frac{\mathrm{Bn}}{G}. \tag{2.22}$$

Since $\delta(t)$ in Eq. (2.15) decreases with time, it will attain the value δ_∞ when $t = t_3$ given by

$$t_3 = \frac{(1 - \mathrm{Bn}/G)^2}{4\alpha^2}. \tag{2.23}$$

In Fig. 2, we have compared the three critical times t_1, t_2 and t_3 as they vary with ratio Bn/G. It is apparent that $t_3 < t_2 < t_1$. Thus, the velocity in the core holds over a time interval less than t_1 found by Safronchik [1].

2.4 Velocity Field in the Yielded Region

We now turn to the determination of the velocity field in the yielded region. This is given by Eqs. (6.1.19) and (6.1.34) in [5], and takes the following form:

$$u(y,t) = Gt + I_1(y,t) + I_2(y,t) + I_3(y,t). \tag{2.24}$$

Here, the $I_j,\ j = 1,2,3$, are integrals with complicated expressions. In the Appendix, we have listed these integrals from Eqs. (6.1.35) - (6.1.37) in [5]. At small t, the yield surface is close to $y = 1$. Since $I_2(y,t)$ and $I_3(y,t)$ approach zero as $y \to 1^-$, we can discard them [1]; see also Eqs. (6.1.44) and (6.1.52) in [5] in this connection.

The above assumption has also been tested by evaluating $I_j(y,t),\ j = 1,2,3$, for various values of Bn and G numerically. These tests have verified that this assumption is reasonable as long as $\delta(t)$ is close to unity. In Fig. 3, noting that the integrals are all negative, the absolute values of $I_j(\delta(t),t),\ j = 1,2,3$, for $\mathrm{Bn} = 1$, $G = 1.2$ have been plotted versus time t up to $t_3 = 0.6997$. For this choice of Bn and G, it is clear that $-I_2$ and $-I_3$ are respectively one and two orders of magnitude less than $-I_1$.

Hence, the velocity field in the yielded region is given by the following approximation:

$$u(y,t) = Gt + I_1(y,t), \quad \delta(t) \le y \le 1, \quad t > 0. \tag{2.25}$$

Consequently, from Eqs. (A.1) and (A.15) in the Appendix, we obtain

$$\begin{aligned} u(y,t) &= G\int_0^t \operatorname{erf}(\beta(y,\sigma))\,d\sigma, \quad \delta(t) \le y \le 1,\ t > 0, \\ &= G[t\ \operatorname{erf}(a/\sqrt{t}) + \frac{2a}{\sqrt{\pi}}\sqrt{t}\ e^{-a^2/t} - \frac{4a^3}{\sqrt{\pi}}\int_{1/\sqrt{t}}^{\infty} e^{-a^2z^2}\,dz] \\ &= G[t\ \operatorname{erf}[(1-y)/2\sqrt{t}] + \frac{(1-y)}{\sqrt{\pi}}\sqrt{t}\ e^{[-(1-y)^2/4t]}] \\ &- G\frac{(1-y)^2}{2}(1-\operatorname{erf}[(1-y)/2\sqrt{t})]). \end{aligned} \tag{2.26}$$

From the above, it follows that the core velocity $u(\delta(t),t)$ is given by

$$u(\delta(t),t) = Gt[\operatorname{erf}(\alpha) + \frac{2\alpha}{\sqrt{\pi}}e^{-\alpha^2} - 2\alpha^2\ \operatorname{erfc}(\alpha)], \tag{2.27}$$

where $\operatorname{erfc}(\cdot)$ is the complementary error function. That is, the velocity in the core is proportional to Gt and does not agree with that given by $u_c(t)$ in Eq. (2.18). The reason lies in the various approximations made to arrive at these two values. In Fig. 4, we have compared the two when the Bingham number $\mathrm{Bn} = 1$, and the pressure drop $G \in \{5, 10, 100\}$. When G is small, the profile of $u_c(t)$ given by Eq. (2.18) depends on $\sqrt{t}$ and is curved, and at large values of G, the linear term is dominant and the profile of $u_c(t)$ is almost linear. In this situation, the core velocities in Eqs. (2.18) and (2.42) are almost identical.

3 Numerical Comparison

Since the velocity field in Eq. (2.26) is difficult to find, one may assume that the velocity field in the yielded region is parabolic, with the size of the core, $\delta(t)$, and the velocity in the core, $u_c(t)$, given by Eqs. (2.15) and (2.18) respectively. That is, the parabolic approximation has the form

$$u(y,t) = a(t) + b(t)y + c(t)y^2, \quad \delta(t) \le y \le 1,\ t \ge 0, \tag{3.1}$$

where the functions $a(t), b(t)$ and $c(t)$ have to be determined. Here, one appeals to the following boundary conditions:

1. The velocity at the boundary is zero. Hence, $u(1,t) = 0 \Rightarrow a(t)+b(t)+c(t) = 0$.

2. The velocity at the yield surface is that of the core. Thus, $u(\delta(t),t) = u_c(t) \Rightarrow a(t) + b(t)\delta(t) + c(t)\delta(t)^2 = u_c(t)$.

3. The shear rate at the yield surface is zero. Or, $\partial u(y,t)/\partial y = 0$ at $y = \delta(t)$. Thus $b(t) + 2c(t)\delta(t) = 0$.

Using the above conditions, we obtain the velocity field in the fluid as follows:

$$u(y,t) = \begin{cases} u_c(t), & 0 \le y \le \delta(t),\ t > 0, \\ \Big[u_c(t)/(1-\delta(t))^2\Big](1-y)[1+y-2\delta(t)], & \delta(t) \le y \le 1,\ t > 0. \end{cases} \tag{3.2}$$

We shall now compare the velocity profile in the yielded region given by Eq. (2.26) with the parabolic approximation in Eq. (3.2). From Eqs. (2.22) and (2.23), we note that $\delta(t_3) = \delta_\infty = \mathrm{Bn}/G$. Hence, in Fig. 5, where $\mathrm{Bn} = 1$ and $G = 10$, one has $\delta(t_3) = \delta_\infty = 0.1$, with $\alpha = 0.9627$ and $t_3 = 0.2185$. In Fig. 6, where $\mathrm{Bn} = 1$ and $G = 100$, we see that $\delta(t_3) = \delta_\infty = 0.01$, with $\alpha = 1/6056$ and $t_3 = 0.09505$. In Figs. 5 and 6, we have plotted 10 velocity profiles corresponding to $t_i = t_3/10$, $i = 1, 2, \cdots, 9$, and $t_{10} = t_3$.

It is clear that the comparisons in Figs. 5 and 6 are not accurate, for the velocity approximation in Eq. (2.26) is based on the assumption that $\delta(t) \approx 1$. Hence, in Figs. 7 - 9, we have compared the velocity profile in Eq. (2.26) with that given by the parabolic approximation in Eq. (3.2) in the time interval $[0, t_{09}]$, where t_{09} is the time at which $\delta(t_{09}) = 0.9$. It turns out that $t_{09} = 0.0025/\alpha^2$. In these figures, we have let $\mathrm{Bn} = 1$, and $G \in \{10, 100, 1000\}$. Again, ten profiles are shown as t increases from $t_1 = 0.1t_{09}$ to $t_{10} = t_{09}$ in equal instalments. The corresponding values of α are $0.0002698, 0.000009698$ and 0.00005601 respectively. It is clear that the parabolic approximation for the velocity field performs well for small Bn/G ratios.

4 Concluding Remarks

For a time interval of short duration, the determination of the velocity profile in the start-up flow of a Bingham fluid in a channel due to a constant pressure gradient is now complete. The earlier work of Safronchik [1] had delivered the location of the yield surface and the velocity in the core; for a summary, see [5]. Here, we have found the velocity in the yielded zone. This exact

solution approximates quite nicely the velocity in the core for high values of the pressure gradient. A comparison of this exact solution with that obtained by a parabolic approximation shows that the two differ from one another at low values of the pressure drop G and converge as G increases.

Finally, solutions to initial boundary value problems in Bingham fluids using the Laplace Transform have appeared in the literature. Using this method, Daprà and Scarpi [7] examined the start-up of channel flow, which is the same as that studied here. Subsequently, they applied the same technique to the start-up flow in a pipe of circular cross-section [8]. More recently, Wu and Liu [9] employed the Laplace transform technique to the start-up flow of a Bingham fluid between coaxial cylinders under a constant wall shear stress. These solutions are incorrect because one cannot use the Laplace transform method for these initial boundary value problems. For a detailed explanation, see Huilgol [10].

Acknowledgements This paper is dedicated to the memory of our friend and colleague, Andreas Alexandrou. We would also like to thank the two reviewers for their helpful suggestions which led to several clarifications and improvements of our manuscript.

References

[1] A. I. Safronchik, Non-steady flow of a visco-plastic material between parallel walls. J. Appl. Math. Mech. (PMM), 23 (1959), 1314–1327.

[2] A. I. Safronchik, Rotation of a cylinder with a variable angular velocity in a visco-plastic medium. J. Appl. Math. Mech. (PMM), 23 (1959), 1504–1511.

[3] A. I. Safronchik, Unsteady flow of visco-plastic material in a circular tube. J. Appl. Math. Mech. (PMM), 24 (1960), 200–207.

[4] K. Sekimoto, An exact non-stationary solution of simple shear flow in a Bingham fluid. J. Non-Newt. Fluid Mech., 39 (1991), 107-113.

[5] R. R. Huilgol, Fluid Mechanics of Viscoplasticity. Springer Verlag, Berlin Heidelberg 2015.

[6] E. W. Ng, M. Geller, A table of integrals of the error function. J. Res. Natl. Bur. Standards - B. Math. Sci., 73B (1969), 1 - 20.

[7] I. Daprà and G. Scarpi, Start-up of channel-flow of a Bingham fluid initially at rest. Rend. Mat. Acc. Lincei, Ser. 9, 15 (2004), 125–135.

[8] I. Daprà and G. Scarpi, Start-up flow of a Bingham fluid in a pipe. Meccanica 40 (2005),49–63.

[9] Y-H. Wu and K-F Liu, Start-up flow of a Bingham fluid between coaxial cylinders under a constant wall shear stress. J. Non-Newt. Fluid Mech., 223 (2015), 116–121.

[10] R. R. Huilgol, "Comments on the paper by Y-H. Wu and K-F Liu : Start-up flow of a Bingham fluid between coaxial cylinders under a constant wall shear stress. Journal of Non-Newtonian Fluid Mechanics 223 (2015), 116-121." J. Non-Newt. Fluid Mech., 244 (2017), 42-43.

Appendix

In this Appendix, we shall list the three integrals $I_1(y,t), I_2(y,t)$ and $I_3(y,t)$, which appear in Eq. (2.24). We begin with [5]

$$\begin{aligned} I_1(y,t) &= \frac{2G}{\sqrt{\pi}} \int_0^t \left(\int_\infty^\beta e^{-\alpha^2}\, d\alpha \right) d\sigma \\ &= -G \int_0^t [1 - \mathrm{erf}(\beta(y,\sigma))]\, d\sigma \\ &= -Gt + G \int_0^t \mathrm{erf}(\beta(y,\sigma))]\, d\sigma, \end{aligned} \tag{A.1}$$

where

$$\beta = \beta(y,\sigma) = \frac{1-y}{2\sqrt{t-\sigma}}, \quad y < 1, \quad t \geq 0. \tag{A.2}$$

We can now evaluate the integral on the right side in Eq. (A.1) as follows. First of all, the error function $\mathrm{erf}(x)$ is defined through

$$\mathrm{erf}(x) = \frac{2}{\sqrt{\pi}} \int_0^x e^{-s^2}\, ds. \tag{A.3}$$

Hence, using integration by parts, we obtain

$$\int \mathrm{erf}(x)\, dx = x\ \mathrm{erf}(x) - \frac{2}{\sqrt{\pi}} \int x\ e^{-x^2}\, dx = x\ \mathrm{erf}(x) + \frac{1}{\sqrt{\pi}} e^{-x^2}. \tag{A.4}$$

Next,

$$\int \mathrm{erf}(az)\, dz = \frac{1}{a} \int \mathrm{erf}(x)\, dx, \tag{A.5}$$

for any constant a. In Eq.(A.5), let

$$a = \frac{1-y}{2}, \quad z = \frac{1}{\sqrt{t-\sigma}}. \tag{A.6}$$

Thus,

$$\frac{dz}{d\sigma} = \frac{1}{2} z^3. \tag{A.7}$$

Hence,

$$\int \mathrm{erf}(\beta(y,\sigma))\, d\sigma = 2 \int \mathrm{erf}(az) z^{-3}\, dz. \tag{A.8}$$

Here, we appeal to the Tables of Integrals due to Ng and Geller [6]. Using Eq. (14) in Section 4.1, we obtain

$$\begin{aligned}\int_0^t \mathrm{erf}(\beta(y,\sigma))\,d\sigma &= 2\int_{1/\sqrt{t}}^{\infty} \mathrm{erf}(az)z^{-3}\,dz \\ = -\lim_{z\to\infty}\left[\frac{\mathrm{erf}(az)}{z^2}\right] &+ t\ \mathrm{erf}(a/\sqrt{t}) + \frac{2a}{\sqrt{\pi}}\int_{1/\sqrt{t}}^{\infty}\frac{1}{z^2}e^{-a^2z^2}\,dz. \end{aligned} \quad (A.9)$$

Since $\mathrm{erf}(az)$ is bounded as $z\to\infty$, the first term goes to zero in the limit. Hence,

$$\int_0^t \mathrm{erf}(\beta(y,\sigma))\,d\sigma = t\ \mathrm{erf}(a/\sqrt{t}) + \frac{2a}{\sqrt{\pi}}\int_{1/\sqrt{t}}^{\infty}\frac{1}{z^2}e^{-a^2z^2}\,dz. \quad (A.10)$$

Next, it is easy to see that

$$\frac{d}{dz}\left[\frac{1}{z}e^{-a^2z^2}\right] = -\frac{1}{z^2}e^{-a^2z^2} - 2a^2e^{-a^2z^2}. \quad (A.11)$$

Thus,

$$\begin{aligned}\frac{2a}{\sqrt{\pi}}\int_{1/\sqrt{t}}^{\infty}\frac{1}{z^2}e^{-a^2z^2}\,dz &= -\frac{4a^3}{\sqrt{\pi}}\int_{1/\sqrt{t}}^{\infty}e^{-a^2z^2}\,dz \\ &- \frac{2a}{\sqrt{\pi}}\lim_{z\to\infty}\left[\frac{e^{-a^2z^2}}{z}\right] + \frac{2a}{\sqrt{\pi}}\sqrt{t}\ e^{-a^2/t}. \end{aligned} \quad (A.12)$$

Since $e^{-a^2z^2}\to 0$ as $z\to\infty$, we obtain

$$\frac{2a}{\sqrt{\pi}}\int_{1/\sqrt{t}}^{\infty}\frac{1}{z^2}e^{-a^2z^2}\,dz = \frac{2a}{\sqrt{\pi}}\sqrt{t}\ e^{-a^2/t} - \frac{4a^3}{\sqrt{\pi}}\int_{1/\sqrt{t}}^{\infty}e^{-a^2z^2}\,dz. \quad (A.13)$$

Next,

$$\frac{2}{\sqrt{\pi}}\int_{1/\sqrt{t}}^{\infty}e^{-a^2z^2}\,dz = \frac{2}{a\sqrt{\pi}}\int_{a/\sqrt{t}}^{\infty}e^{-x^2}\,dx = \frac{1}{a}\left[1-\mathrm{erf}(a/\sqrt{t})\right]. \quad (A.14)$$

Consequently,

$$\begin{aligned} G\int_0^t \mathrm{erf}(\beta(y,\sigma))\,d\sigma &= G[t\ \mathrm{erf}(a/\sqrt{t}) + \frac{2a}{\sqrt{\pi}}\sqrt{t}\ e^{-a^2/t} - \frac{4a^3}{\sqrt{\pi}}\int_{1/\sqrt{t}}^{\infty}e^{-a^2z^2}\,dz] \\ = G[t\ \mathrm{erf}[(1-y)/2\sqrt{t}] &+ \frac{(1-y)}{\sqrt{\pi}}\sqrt{t}\ e^{[-(1-y)^2/4t]}] \\ -G\frac{(1-y)^2}{2}(1 &- \mathrm{erf}[(1-y)/2\sqrt{t}]), \quad \delta(t)\le y\le 1,\ t>0. \end{aligned} \quad (A.15)$$

We now turn to the other two integrals in Eq. (2.24). First of all, I_2 is given by (Huilgol [5])

$$I_2(y,t) = -\frac{1}{\sqrt{\pi}} \int_0^t \phi'(\sigma) \left(\int_{z_1(y,t)}^{z_1(y,\sigma)} e^{-\beta^2} d\beta \right) d\sigma, \tag{A.16}$$

where

$$z_1(y,\sigma) = \frac{y - \delta(\sigma)}{2\sqrt{t-\sigma}}, \tag{A.17}$$

and the lower limits are given by

$$z_1(y,t) = \begin{cases} \infty, & y > \delta(t), \\ 0, & y = \delta(t), \\ -\infty, & y < \delta(t). \end{cases} \tag{A.18}$$

We recall from Eq. (2.15) that

$$\delta(t) = 1 - 2\alpha\sqrt{t}. \tag{A.19}$$

Thus,

$$z_1(\delta(t),\sigma) = -\frac{\alpha(\sqrt{t} - \sqrt{\sigma})}{\sqrt{t-\sigma}} \leq 0. \tag{A.20}$$

Hence, noting that when $x < 0$, one has $\operatorname{erf}(x) = -\operatorname{erf}(-x)$, we obtain

$$\begin{aligned} I_2(\delta(t),t) &= -\frac{1}{\sqrt{\pi}} \int_0^t \phi'(\sigma) \left(\int_0^{z_1(\delta(t),\sigma)} e^{-\beta^2} d\beta \right) d\sigma, \\ &= \frac{1}{2} \int_0^t \phi'(\sigma) \ \operatorname{erf}(-z_1(\delta(t),\sigma))\, d\sigma, \end{aligned} \tag{A.21}$$

where [5]

$$\phi'(\sigma) = -\frac{\mathrm{Bn}}{\delta(\sigma)} = -\frac{\mathrm{Bn}}{1 - 2\alpha\sqrt{\sigma}}. \tag{A.22}$$

Unlike $I_1(y,t)$, we have been unable to evaluate $I_2(y,t)$ analytically.

Next,

$$I_3(y,t) = \frac{1}{\sqrt{\pi}} \int_0^t \phi'(\sigma) \left(\int_{z_2(y,t)}^{z_2(y,\sigma)} e^{-\beta^2} d\beta \right) d\sigma, \tag{A.23}$$

where

$$z_2(y,\sigma) = \frac{2 - y - \delta(\sigma)}{2\sqrt{t-\sigma}}, \tag{A.24}$$

and

$$z_2(y,t) = \begin{cases} \infty, & y > \delta(t), \\ 0, & y = \delta(t), \\ -\infty, & y < \delta(t). \end{cases} \tag{A.25}$$

Now,

$$z_2(\delta(t),\sigma) = \frac{\alpha(\sqrt{t}+\sqrt{\sigma})}{\sqrt{t-\sigma}} \geq 1. \tag{A.26}$$

Thus, one can derive

$$\begin{aligned} I_3(\delta(t),t) &= \frac{1}{\sqrt{\pi}} \int_0^t \phi'(\sigma) \Big(\int_0^{z_2(\delta(t),\sigma)} e^{-\beta^2} d\beta \Big) d\sigma, \\ &= \frac{1}{2} \int_0^t \phi'(\sigma)\ \mathrm{erf}(z_2(\delta(t),\sigma))\, d\sigma. \end{aligned} \tag{A.27}$$

Once again, we have been unable to evaluate $I_3(y,t)$ analytically.

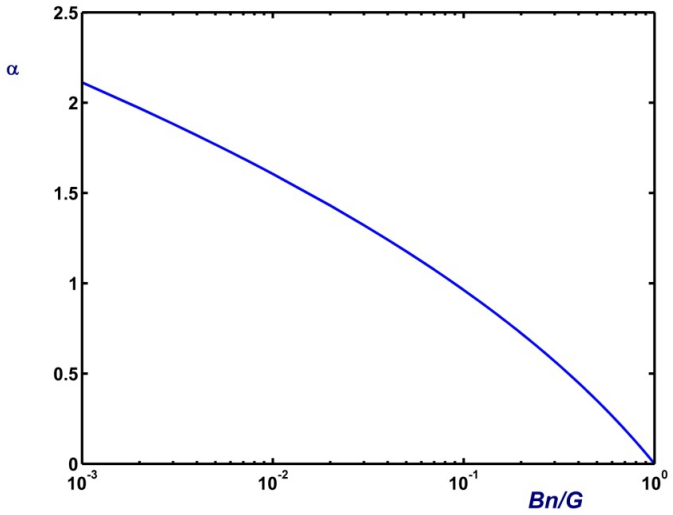

Figure 1. The parameter α as a function of the ratio Bn/G

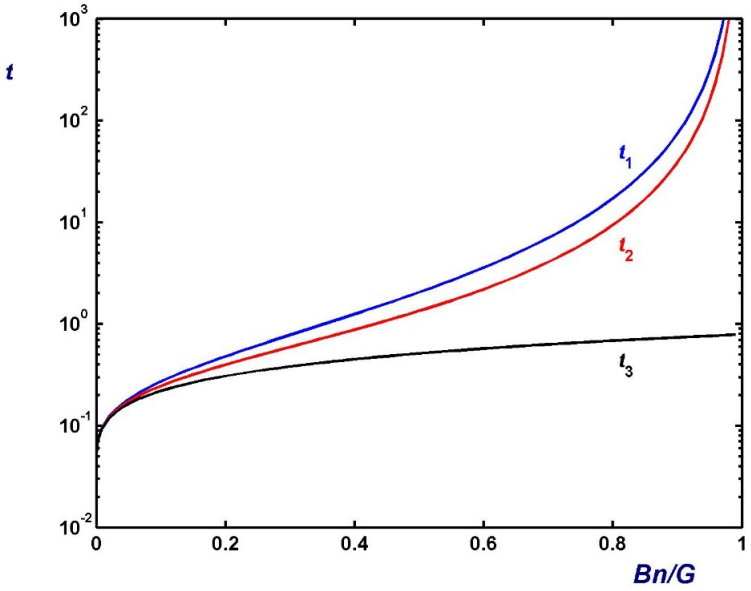

Figure 2. The three critical times t_1, t_2 and t_3 versus the ratio Bn/G

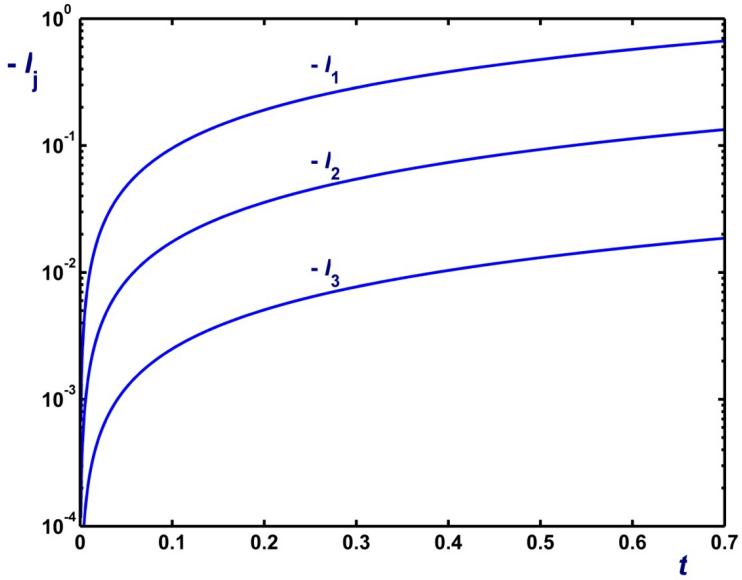

Figure 3. The plots of for Bn=1 and G=1.2. For this choice of parameters, **,** , and .

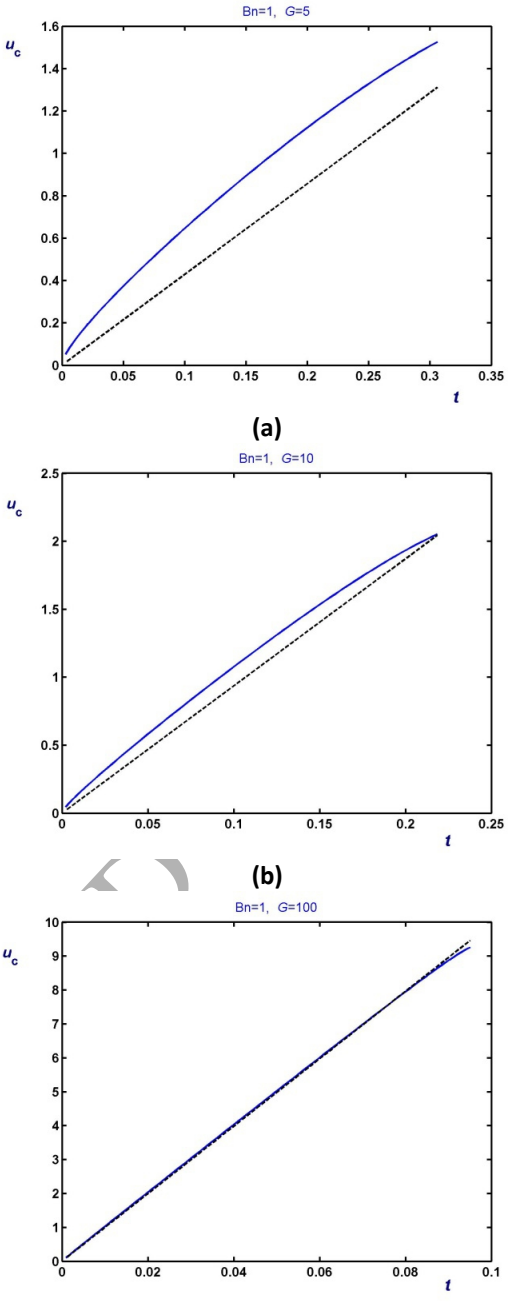

Figure 4. Comparisons of the core velocity predicted by Eq. (2.18) (solid line) and Eq. (2.42) (dashed) line for Bn = 1: (a) $G = 5$ ($\alpha = 0.7231$); (b) $G = 10$ ($\alpha = 0.9627$); $G = 100$ ($\alpha = 1.6056$).

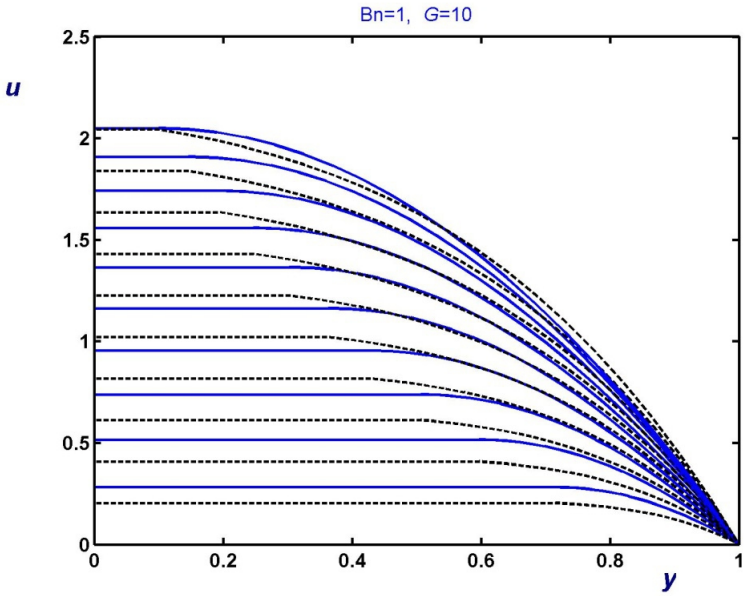

Figure 5. Evolution of the velocity in the interval [0, t_3] for Bn = 1 and G = 10 using the parabolic approximation (3.1) (solid lines) and approximation (2.41) for the velocity (dashed lines).

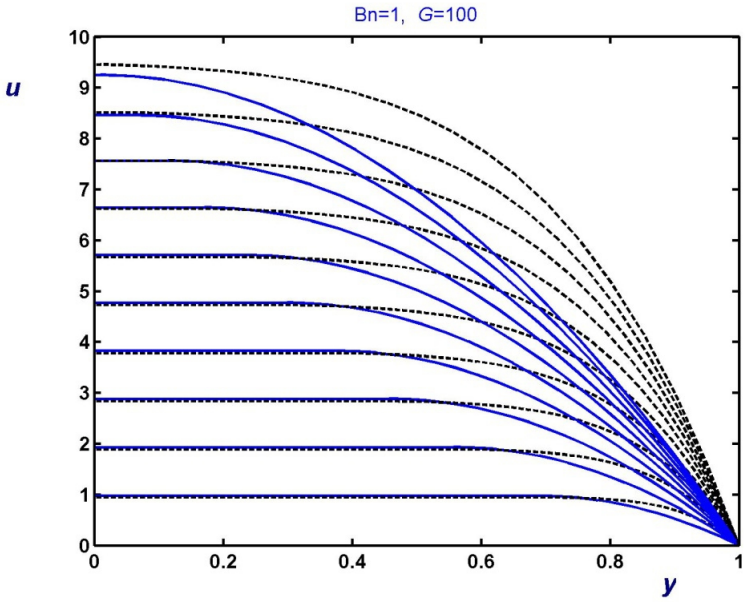

Figure 6. Evolution of the velocity in the interval [0, t_3] for Bn =1 and G = 100 using the parabolic approximation (3.1) (solid lines) and approximation (2.41) for the velocity (dashed lines).

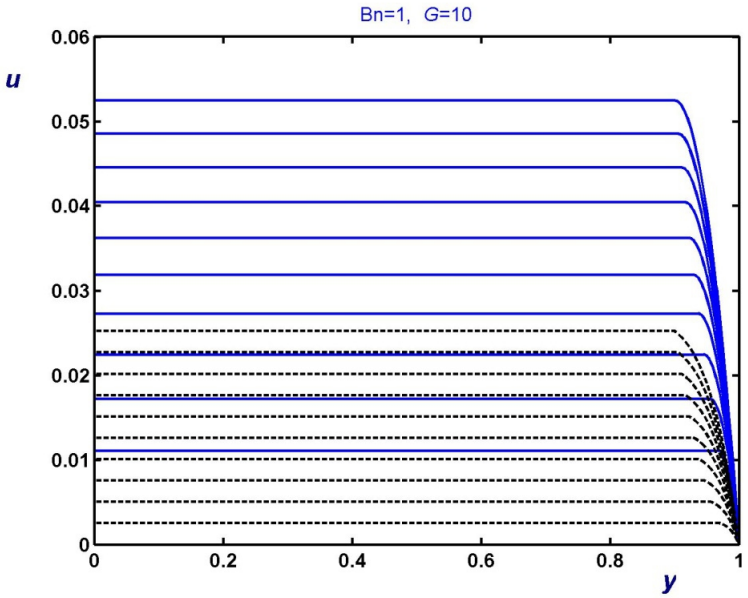

Figure 7. Evolution of the velocity in the interval [0, t_{09}] for Bn =1 and G = 10 using the parabolic approximation (3.1) (solid lines) and approximation (2.41) for the velocity (dashed lines).

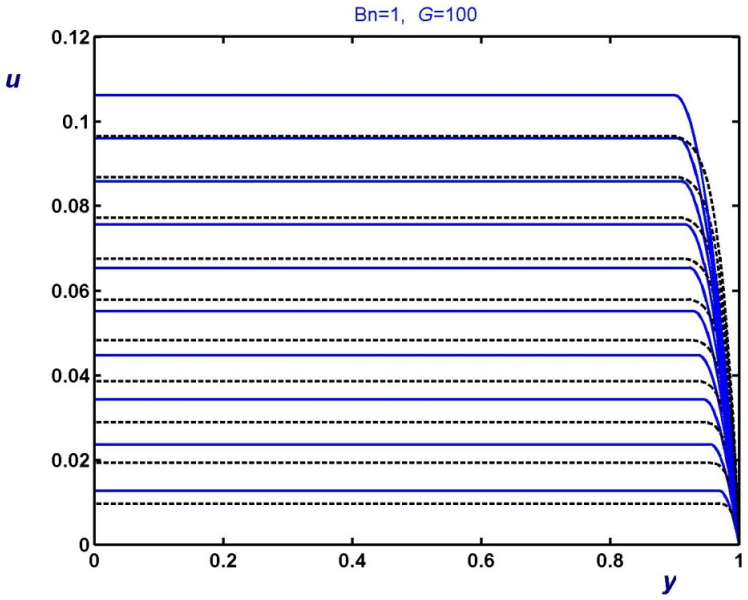

Figure 8. Evolution of the velocity in the interval [0, t_{09}] for Bn =1 and G = 100 using the parabolic approximation (3.1) (solid lines) and approximation (2.41) for the velocity (dashed lines).

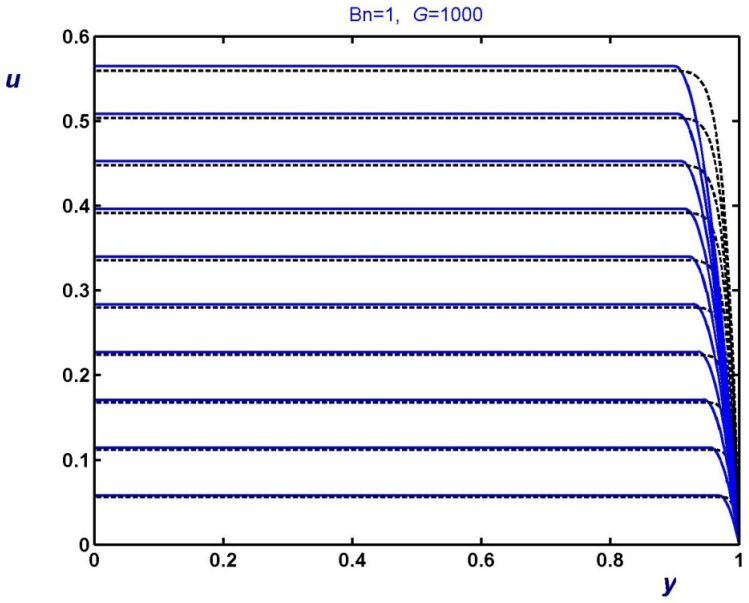

Figure 9. Evolution of the velocity in the interval $[0, t_{09}]$ for Bn =1 and $G = 1000$ using the parabolic approximation (3.1) (solid lines) and approximation (2.41) for the velocity (dashed lines).